ARTICLE

https://doi.org/10.1590/2317-488920202020190113

BJGEO Brazilian Journal of Geology

# Inversion of satellite gravimetric data from Recôncavo-Tucano-Jatobá Basin System

Thaíza Pereira Bessoni[1], Amin Bassrei[1,2*], Luiz Gabriel Souza de Oliveira[3]

## Abstract

Density differences among subsurface rocks cause variations in the gravitational field of Earth, which is known as gravity anomaly. Interpretation of these gravity anomalies allows assessment of the probable depth and shape of the causative body. For several decades, gravity data were acquired on the surface, but after the scientific and technological advances of the last decades, geopotential models were developed, including gravitational observations on a global scale through space satellite missions. This paper investigated the Moho structure in the region of Recôncavo-Tucano-Jatobá rift-basin system based on the information of the terrestrial gravity field from the EIGEN-6C4 geopotential model. The frequency domain inversion technique was applied, which is known as the Parker-Oldenburg iterative method. Bouguer anomaly data were used in the inversion procedure to determine the thickness and geometry of the crust in the region. Data inversion considered a two-layer model with constant density contrast, in which the entire signal was related to Moho topography. In addition, data inversion was carried out to determine the basement depths. The program proved to be efficient and able to manage large data sets. The results, both of the crust thickness and the sedimentary package, validated the geodynamic evolution understanding of the basin system.

**KEYWORDS:** gravity inversion; satellite data; Parker-Oldenburg method; geopotential model EIGEN-6C4; gravity field and steady-state ocean circulation explorer.

## INTRODUCTION

A classic problem of Geophysics is the subsurface determination of a density interface geometry associated with a gravitational anomaly, for instance, the mapping of Mohorovičić (or Moho) discontinuity. In this case, the objective is to invert the gravity anomaly, which is usually filtered, to obtain the interface geometry. Several authors have presented different algorithms for calculating the density interface geometry related to a known gravity anomaly. Cordell and Henderson (1968), Dyrelius and Vogel (1972) used an approximation of the disturbing body through various rectangular prisms of constant density. The gravity effect for each prism was calculated and then the total gravitational field was determined by adding the effect of all prisms. When the model is complicated or when a large number of observations are available, this process can be computationally time-consuming as the number of operations increases greatly with the product of the number of observations and points defining the model.

Parker (1972) showed that a sum of Fourier transforms can be used to calculate the magnetic or gravitational anomaly caused by an irregular layer with constant density. The Fast Fourier Transform (FFT), along with advances in computer technology, has made Parker's method feasible for fast computation of magnetic and gravity fields. Oldenburg (1974) demonstrated that Parker's expression can be inverted to determine the density interface geometry from the gravitational anomaly. Nagendra *et al.* (1996) presented a FORTRAN language computer program based on the Parker-Oldenburg method for analyzing 2D gravity data. Finally, Gómez-Ortiz and Agarwal (2005) presented a MATLAB language-based program for the 3D extension of the Parker-Oldenburg method to obtain the density interface geometry.

These last developments in data modeling and inversion and use of satellite data stimulated new results in Moho mapping. In the recent years, several researchers studied this problem at a regional scale. Braitenberg *et al.* (2000) studied Moho depths in the Tibet region. They used an iterative methodology to invert gravity data and obtain the 3D variation in Moho depth. The gravity inversion was constrained by results from deep seismic sounding and seismological investigations. They found Moho between 70 and 75 km depth over most of the Tibet. Ebbing *et al.* (2013) used satellite gravity gradients to study the regional geology in the Arabian Peninsula. In addition to satellite gravity gradients, they have used terrestrial data sets and global models like EGM2008. Sampietro (2015) retrieved the Moho depth from the Gravity field and steady-state Ocean Circulation Explorer (GOCE). Such investigator used a Bayesian classification algorithm with an iterative Wiener filter to infer information on the crustal structure in the Western Balkan area. The resulting Moho depth ranges

[1]Universidade Federal da Bahia – Salvador (BA), Brazil. E-mails: thaizabessoni@gmail.com, bassrei@ufba.br

[2]Instituto Nacional de Ciência e Tecnologia de Geofísica de Petróleo – Salvador (BA), Brazil.

[3]Universidade Federal do Espírito Santo – São Mateus (ES), Brazil. E-mail: luiz.g.oliveira@ufes.br

*Corresponding author.

between about 20 km beneath the Adriatic Sea and 45 km in the Dinarides. In the search for shallower sources, Paoletti *et al.* (2014) inverted the gravity field of the Neapolitan Volcanic Area, using a technique called depth-resolution plot based on a well-known singular value decomposition technique.

On a global scale we mention the work of Sjöberg (2009), which dealt with the inverse problem in isostasy in order to obtain Moho depth from known Bouguer gravity anomalies and a reference Moho depth. His theoretical approach was formulated to iteratively solve a non-linear Fredholm integral equation of the first kind, also proving the solution uniqueness. More recently, Reguzzoni and Sampietro (2015) used GOCE data to estimate a new crustal model called GOCE Exploitation for Moho Modeling and Applications (GEMMA). Their iterative algorithm, which has been computed at a spatial resolution of 0.5 × 0.5 degree, provided an improved model in terms of resolution and consistent with other global models.

This paper investigates the crustal structure in the region of Recôncavo-Tucano-Jatobá rift-basin system, determining the thickness and geometry of the crust in the region through data inversion by the Parker-Oldenburg iterative method, as presented by Gómez-Ortiz and Agarwal (2005). Based on the knowledge of the average depth of the density interface and the density contrast between the two media, the 3D interface geometry has been calculated iteratively. The iterative process ends when the root mean square (RMS) deviation between two successive approximations is lower than a previously chosen value; and the RMS deviation is therefore used as a convergence criterion. Besides that, the iterative process ends when a maximum number of iterations, also previously chosen, are reached. A low-pass filter in the frequency domain has been incorporated to improve convergence in the iterative process. The gravitational anomaly data used in this paper were obtained from the ICGEM database of the German Geoscience Research Center or GFZ from GeoForschungsZentrum, located in Potsdam, Germany. We have also investigated the sedimentary thickness in the same rift-basin system area. The results are in accordance with the literature, both for the crust thickness and for the sedimentary package.

As far as the issue of uniqueness is concerned, Sampietro and Sanso (2012) investigated the inverse gravimetric problem, which is, in general, known to have a very large indeterminacy. However, they proved that when density models are strongly reduced to simple classes, the uniqueness property of the inversion is retrieved. Uniqueness theorems were proved for three simple cases, in which one case was the recovery of the interface between two layers of known density, as in the present study.

One important feature is the algorithm capability of handling large data sets, which require the use of direct and inverse Fourier transforms.

## METHODOLOGY AND INVERSION PROCESS

The inversion procedure uses the equation described by Parker (1972) to calculate the gravity anomaly caused by an irregular layer of constant density through a series of Fourier transforms. This expression, in its 1D form, is defined as (Eq. 1):

$$\mathcal{F}[\Delta g] = -2\pi G\Delta\rho e^{-kz0}\sum_{n=1}^{\infty}\frac{k^{n-1}}{n!}\,\mathcal{F}\left[h^n(\vec{r})\right] \quad (1)$$

In which:
$F[\Delta g]$ = the Fourier transform of the gravity anomaly;
$G$ = the gravitational constant;
$\Delta\rho$ = the density contrast across the interface;
$k$ = the wave number;
$h^n(\vec{r})$ = the $n$-th power of the interface depth (positive towards down);
$z_0$ = the average depth of the horizontal interface.

Parker (1972) departed from the Fourier transform definition of the potential obtaining the expression given by Equation 1, which is a sum of Fourier transforms.

Oldenburg (1974) reorganized Equation 1 to calculate the depth for the undulated interface of the gravitational anomaly profile through an iterative process. The result is given by Equation 2:

$$\mathcal{F}[h(x)] = -\frac{\mathcal{F}[\Delta g(x)]e^{kz_0}}{2\pi G\Delta\rho} - \sum_{n=2}^{\infty}\frac{k^{n-1}}{n!}\mathcal{F}[h^n(x)] \quad (2)$$

This expression enables determining the density interface of the topography by means of an iterative inversion procedure. Because the Bouguer anomaly only depicts the lateral density contrasts, the position vector $\vec{r}$ can be replaced by $x$, resulting in $h(x)$. In this procedure, the average interface depth, $z_0$, as well as the density contrast associated with the two media, $\Delta\rho$, are assumed to be known. Figure 1 shows the topography and densities for an illustrative example with a two-layer undulating medium wave.

The first term of Equation 2 has been calculated by assigning $h(x) = 0$, so that the inverse Fourier transform of this quantity provides an updated value for the topography $h(x)$. During this step, a filtering procedure occurs in the spatial frequency domain as illustrated in Equation 3:

$$\mathcal{F}[h(x)=0] = F(k_0) \rightarrow [FILTER] \rightarrow \mathcal{F}^{-1}[F(k_0)] = h_1(x) \quad (3)$$

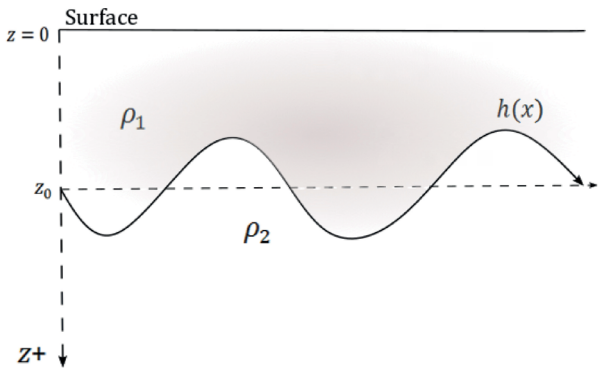


**Figure 1.** Illustrative sketch of the function that defines the interface between two layers with $\rho_1$ and $\rho_2$ densities.

The value of $h_1(x)$ is then entered back into Equation 2 to generate a new estimate of $h(x)$ (Eq. 4):

$$\mathcal{F}\left[h_1(x)\right]=F(k_1)\rightarrow\left[FILTER\right]\rightarrow\mathcal{F}^{-1}\left[F(k_1)\right]=h_2(x) \quad (4)$$

The RMS deviation value between the new and the previous topographies is computed by the expression (Eq. 5):

$$RMS=\sqrt{\frac{\sum\left[h_n(x)-h_{n-1}(x)\right]^2}{\left[2\times(N_r\times N_c)\right]}} \quad (5)$$

In which:
$N_r$ = the number of rows;
$N_c$ = the number of columns in the data array.

The iterative process ends when the maximum of 10 iterations is reached, or, as a convergence criterion, when the difference between two successive approximations of the topography is smaller than a previously chosen value.

According to Oldenburg (1974), the process is convergent if the depth to the interface is greater than zero and does not intersect the topography. In addition, the interface relief amplitude must be lower than the average interface depth.

The instability behavior in the high frequency range will be dealt by means of the mentioned filter, which cuts the high frequencies, that is, it is a low-pass filter denoted by $HFC(k)$. High frequency oscillations related to the shallower sources can be eliminated by multiplying the right side of Equation 2 by the expression (Eq. 6):

$$HCF(k)=\begin{cases}0, & \text{if } \dfrac{k}{2\pi}>SH,\\ \dfrac{1}{2}\left[1+\cos\left(\dfrac{k-2\pi WH}{2(SH-WH)}\right)\right], & \text{if } WH\le\dfrac{k}{2\pi}\le SH,\\ 1, & \text{if } \dfrac{k}{2\pi}<WH,\end{cases} \quad (6)$$

The filter passes all frequencies up to $WH$ and does not pass any above the cutoff frequency $SH$. The intermediate frequencies between $WH$ and $SH$ depend on Equation 6, as shown in the illustrative case of Figure 2. The $WH$ and $SH$ frequency values are chosen to constrain the high frequency content in the Fourier spectrum of the observed gravity anomaly, improving the series convergence.

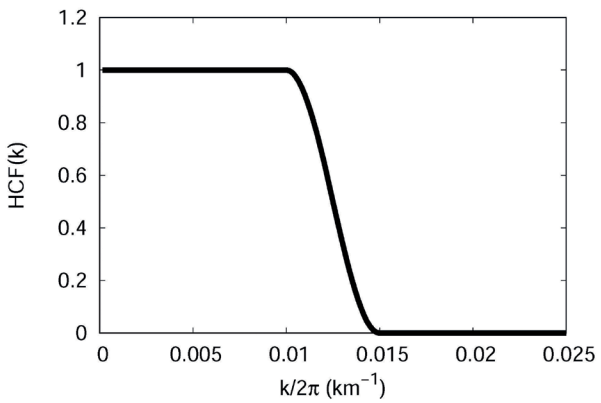


**Figure 2.** Low-pass filter, $HCF(k)$, with $WH$ = 0.01 km$^{-1}$ and $SH$ = 0.015 km$^{-1}$.

Because the topographic relief is determined in the inversion procedure, it is desirable to calculate the gravity anomaly produced by this topography, which was performed by Equation 1. With the process convergence, the predicted or calculated anomaly is similar to the observed anomaly, and the latter is used as input to the inversion process (Gómez-Ortiz and Agarwal 2005).

The software requires that the following parameters used in the process be supplied to the program:

- name of the input file containing the observed gravity anomaly data (in milligal), for example, bouguer.dat;
- name of the output file with the depths (in km) of the surface that generates the anomaly as a result of the inversion, for example, topooutput.dat;
- output file name with calculated anomaly (in milligal), for example, bouinv.dat;
- number of rows and columns;
- length of the data mesh (in km) in $x$ and $y$ directions, as in Longx and Longy;
- density contrast: $\Delta\rho$ (g/cm$^3$);
- average interface depth, $z_0$ (km);
- convergence criterion expressed as the value of the RMS deviation between two successive approximations of the topography (in km); and (9) frequency values for the low-pass filter: $WH$ and $SH$ (km$^{-1}$).

At the end of the iterative process, the program provides information to make three graphics: estimated topography; predicted gravity anomaly, due to the estimated topography, calculated from Equation 1, and residual between the observed and predicted gravity anomalies. The value of the RMS topography deviation between the iterations and the iteration number at which the process stopped are also provided.

## Data and geology of the area

Global gravitational field models, especially those derived from satellite measurements, have become increasingly detailed and accurate (Barthelmes 2009). The data used come from the combined gravity field model EIGEN-6C4, which is the fourth version of the EIGEN-6C, and EIGEN stands for European Improved Gravity model of the Earth by New techniques. The EIGEN-6C4 is composed of a combination of gravitational data from GOCE satellite; data from previous satellite missions; terrestrial data and also radar altimetry data. These data can be obtained from the ICGEM database, which is the International Center for Global Earth Models of the German GFZ Potsdam Geo-research Center. Gravitational anomaly data from Earth, already with the Bouguer correction, were downloaded with a 2' arc grid spacing. An extrapolation of the area of interest was considered in order to attenuate the edge effect in this region during the inversion procedure.

Recôncavo-Tucano-Jatobá rift-basin system is located near the coast of the Northeast Region of Brazil and extends from the State of Bahia to the State of Pernambuco. Its formation is related to an aborted rift from the continental separation

between South America and Africa during the Mesozoic, which then generated the South Atlantic Ocean. The system is formed by three basins, known as Recôncavo, Tucano e Jatobá, represented in Figure 3. The system is limited to the South by the Camamu Basin, to the West by the Itabuna-Salvador-Curaçá Block, the Serrinha Block, and the Sergipana Range, and the Pernambuco-Alagoas Massif. It is bordered to the East by Salvador-Esplanada Belt, Sergipana Belt, and Pernambuco-Alagoas Massif, and bordered to the North by Pernambuco Shear Zone (Silva 2017).

Figure 4 shows the Bouguer gravity anomaly map associated with the mantle-crust boundary in Recôncavo-Tucano-Jatobá rift region. The region in question is shown delimited by the white line. The strongest signature of the Bouguer anomaly is the negative gradient within the continent, but one can see prominent lows of gravity throughout Recôncavo-Tucano-Jatobá rift-basin system. The negative peak is approximately -150 mGal within Tucano Central Sub-basin.

As a map of gravimetric anomalies is composed of the sum of shallow and deep sources, it is necessary to separate local and shallow anomalies from deep and regional anomalies. In practical terms, the regional component must contain the sources of the crust/mantle interface, which is our interest. On the other hand, the residual component must contain anomalies with sources in the crust. The separation of data into its regional and residual components was done by applying the upward continuation filter (Blakely 1996, p. 313). Hence, a desired level of smoothing is achieved, maintaining only the information on the severity anomaly associated with the crust-mantle limit. Figure 5 shows the Bouguer gravity anomaly map with the application of the continuation filter above 20 km. The most accentuated signature of the Bouguer anomaly is its negative gradient within the continent. Prominent gravity lows can be observed throughout the Recôncavo-Tucano-Jatobá onshore basin, reaching approximately -95 mGal within the Central Tucano Sub-basin.

Recôncavo Basin occupies an area of approximately 11,500 km$^2$. Exploratory efforts over decades to date have resulted in regional surveys of gravimetric and magnetometric data, 2D and 3D seismic data acquisition, and 6,725 wells (May 2017 data), of which 1,263 are exploratory. Basin is the segment of an interrupted intracontinental rift and its basic architecture reflects a NE-SW oriented semi-graben (Prates and Fernandez 2015). According to Abrahão and Warme

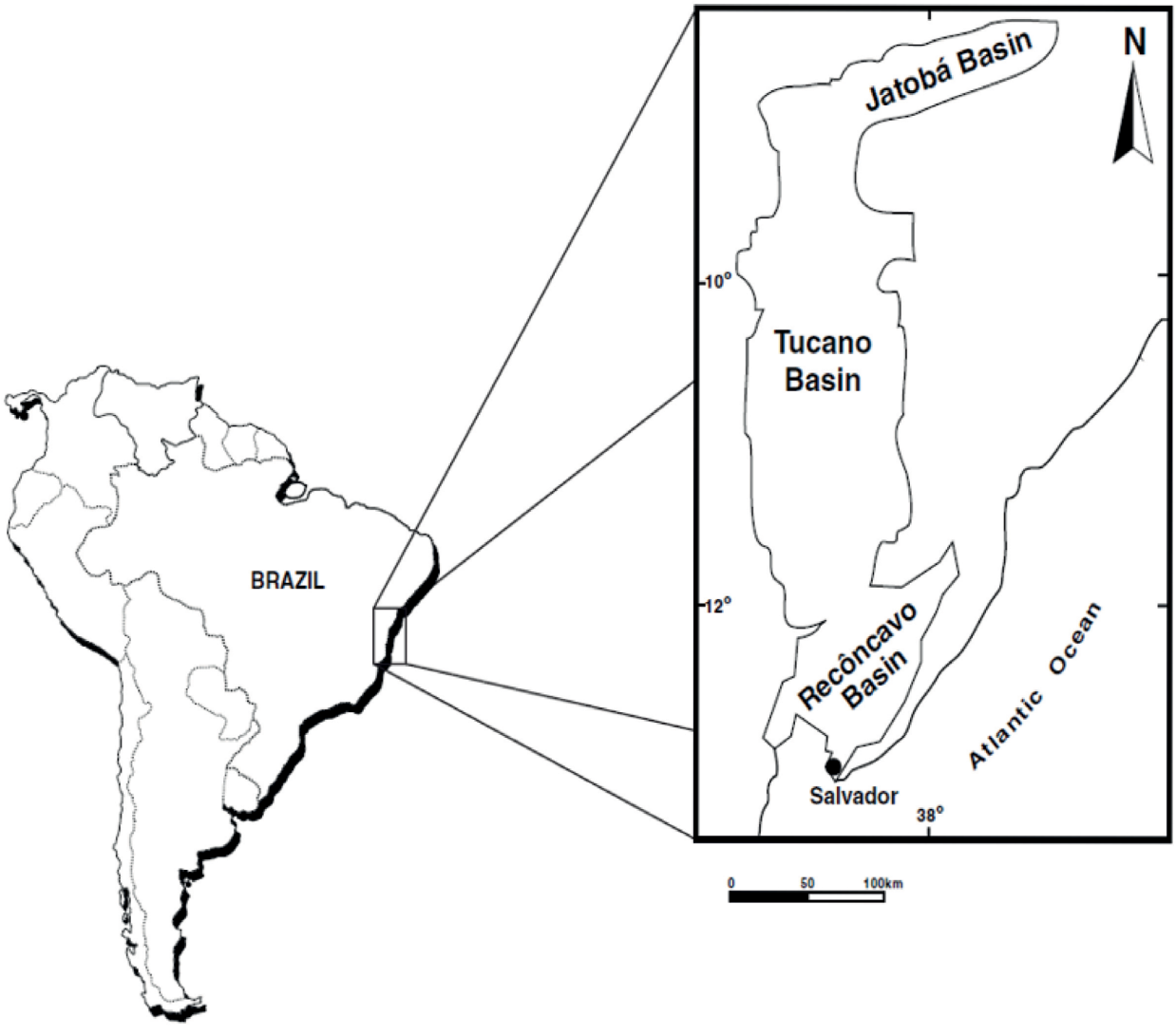


**Figure 3.** Location map of the area of interest, based on Magnavita (2000).

(1990), the stress field responsible for the rifting would have acted between the Meso-Jurassic and the Eocretaceous. According to Magnavita (1992), the preserved sedimentary section in the Recôncavo Basin has a maximum thickness of the order of 6,900 m, in the Camaçari Low area. In addition, based on Santos *et al.* (1990), the sedimentary thickness in the Recôncavo is more than 6,000 m wide.

Tucano Basin is in the Northeast of the State of Bahia, occupying an area of approximately 30,500 km$^2$. Structural features with NW-SE direction allow subdividing it into Tucano South, Tucano Central, and Tucano North Sub-basins. To the North, Tucano Central separates from Tucano North by Vaza-Barris Zone. To the South, the boundary between the Tucano South Sub-basin and Recôncavo Basin is given by Alto de Aporá. To the East, the Faults of Inhambupe and Adustina constitute, respectively, the boundaries of Tucano South and Tucano Central Sub-basins (Magnavita 1992). The boundary of Tucano

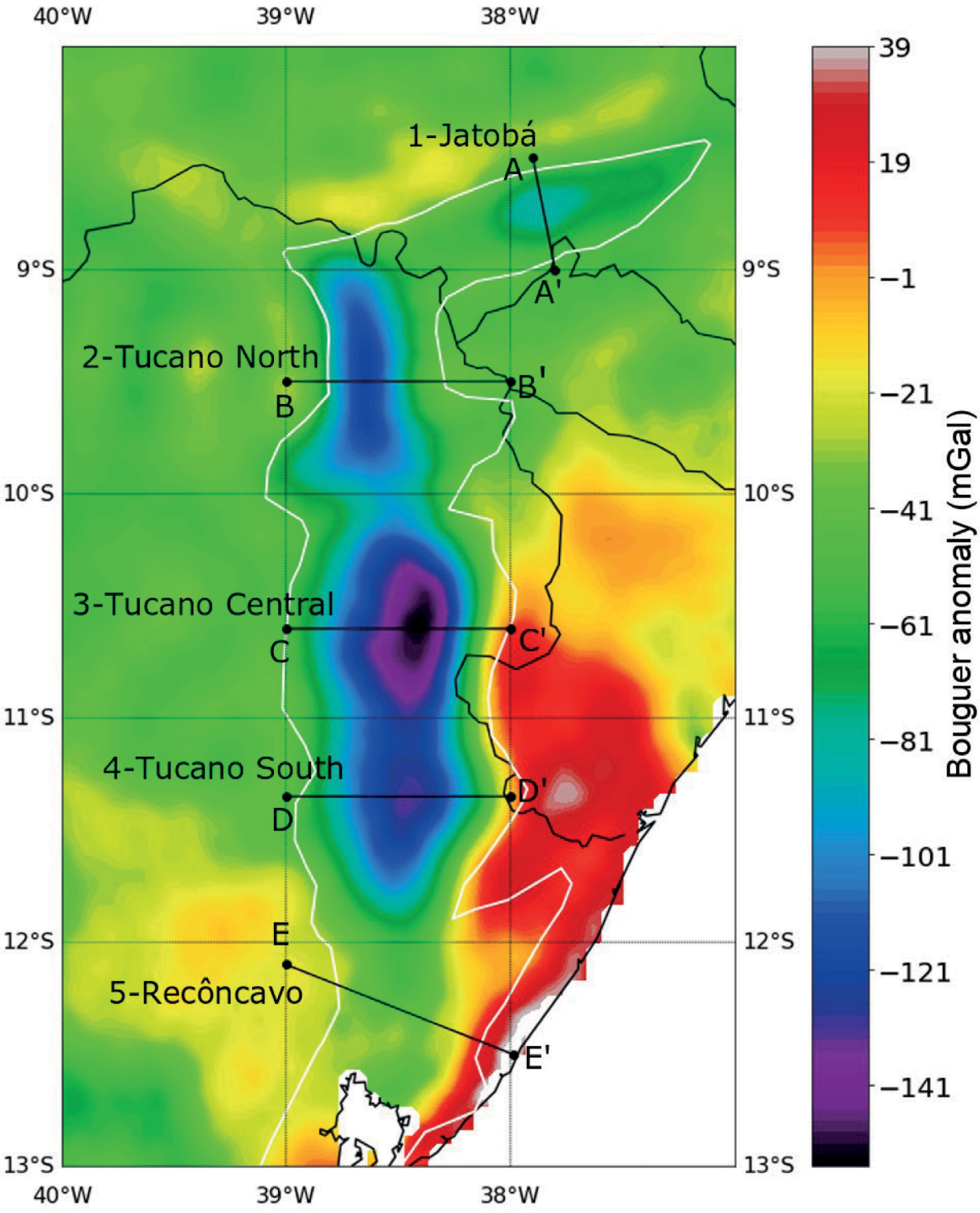


**Figure 4.** Bouguer anomaly map of Recôncavo-Tucano-Jatobá rift-basin system. The outline of the rift shape, represented by the white line, was based on Magnavita (1992).

North Sub-basin with the Jatobá Basin is given by São Francisco Fault to the Northeast. The basement estimated depths in the depocenter are over 6,000 m for the Tucano South Sub-basin and approximately 8,000 m for the Tucano Central Sub-basin (Cícero Dantas Low). For the Tucano North Sub-basin, in Salgado do Melão Low, the estimated depths are around 6,000 m (Magnavita 1992).

Jatobá Basin occupies an area of approximately 5,000 km$^2$ with NE-SW orientation. São Francisco Faults to the West and Ibimirim to the North constitute its main structural boundaries. To the South and East, their contact with the basement is discordant or occurs through minor faults. The change in the opening direction of the rift from S-N in Tucano North to SW-NE in Jatobá Basin may be the most explicit example of the control exerted by past basement structures. This inflection is conditional on the Pernambuco-Paraíba Shear Zone, whose reactivation during the Eocretaceous led to Ibimirim Fault, the Northern boundary of Jatobá Basin (Santos *et al.* 1990, Magnavita 1992). The basement estimated depth in Ibimirim Low is around 4,000 m (Magnavita 1992).

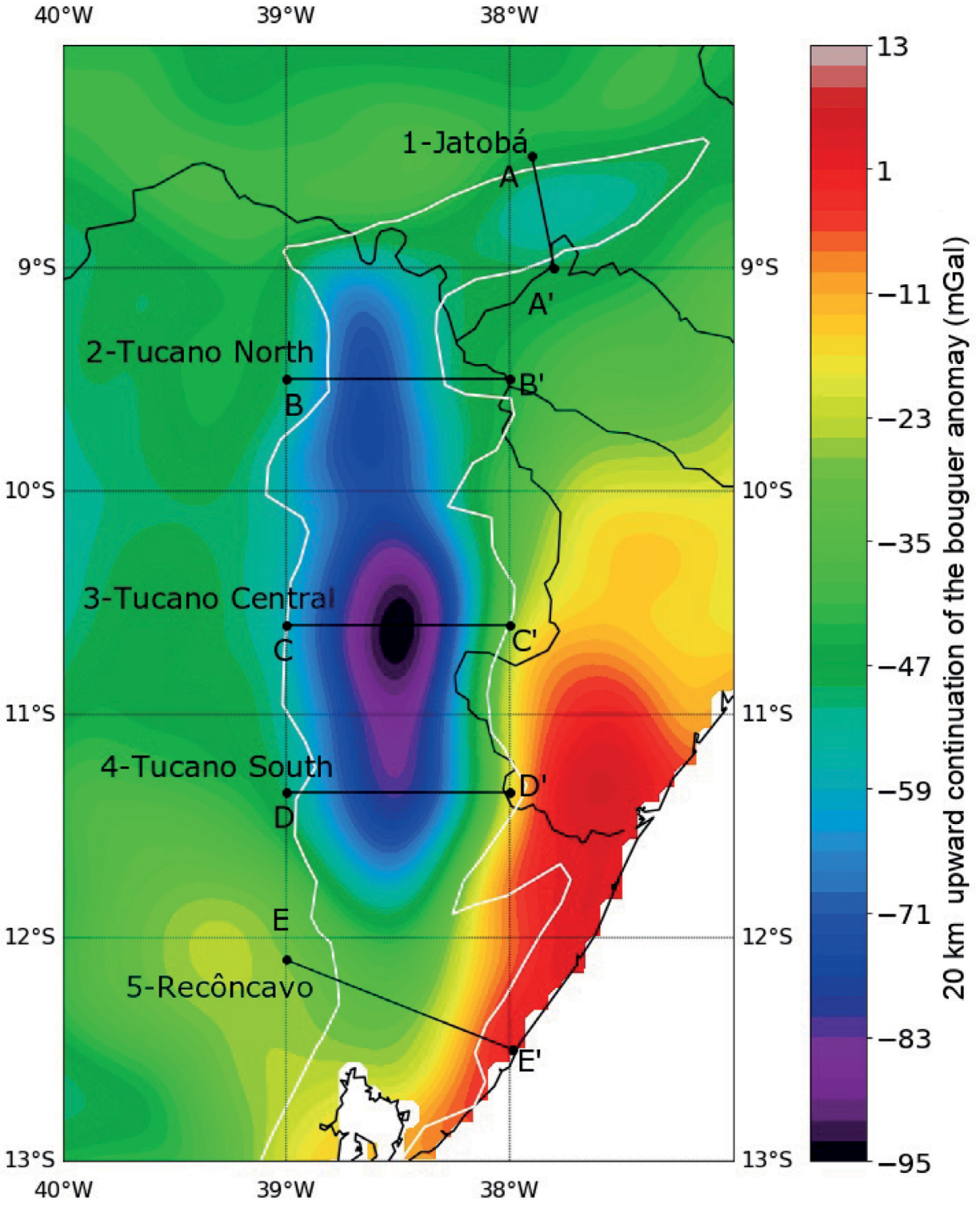


**Figure 5.** Bouguer anomaly map of Recôncavo-Tucano-Jatobá rift-basin system after the 20 km upward continuation filter.

## RESULTS AND DISCUSSION

Moho topography under Recôncavo-Tucano-Jatobá rift-basin system derived from satellite gravity inversion is shown in Figure 6. Tucano Central Sub-basin shows the crust thicker than the other basins, somewhere around 33 to 35 km, followed by the Tucano South Sub-basin, which is approximately 33 km deep. Further South is Recôncavo Basin, with a maximum crustal thickness of 29 km. In Tucano North Sub-basin, Moho appears to be close to 32 km. And finally, under the Jatobá Basin, the crust/mantle interface is around 30 km. For a more detailed representation of such estimates, five profiles were chosen (Fig. 7), which cut the center of each of the rift constituent basins. The location at which each profile was drawn is shown in Figure 6. The E – E' profile clearly shows that the Moho under Recôncavo Basin is not as prominent as in the other basins. Blaich *et al.* (2008) performed gravity

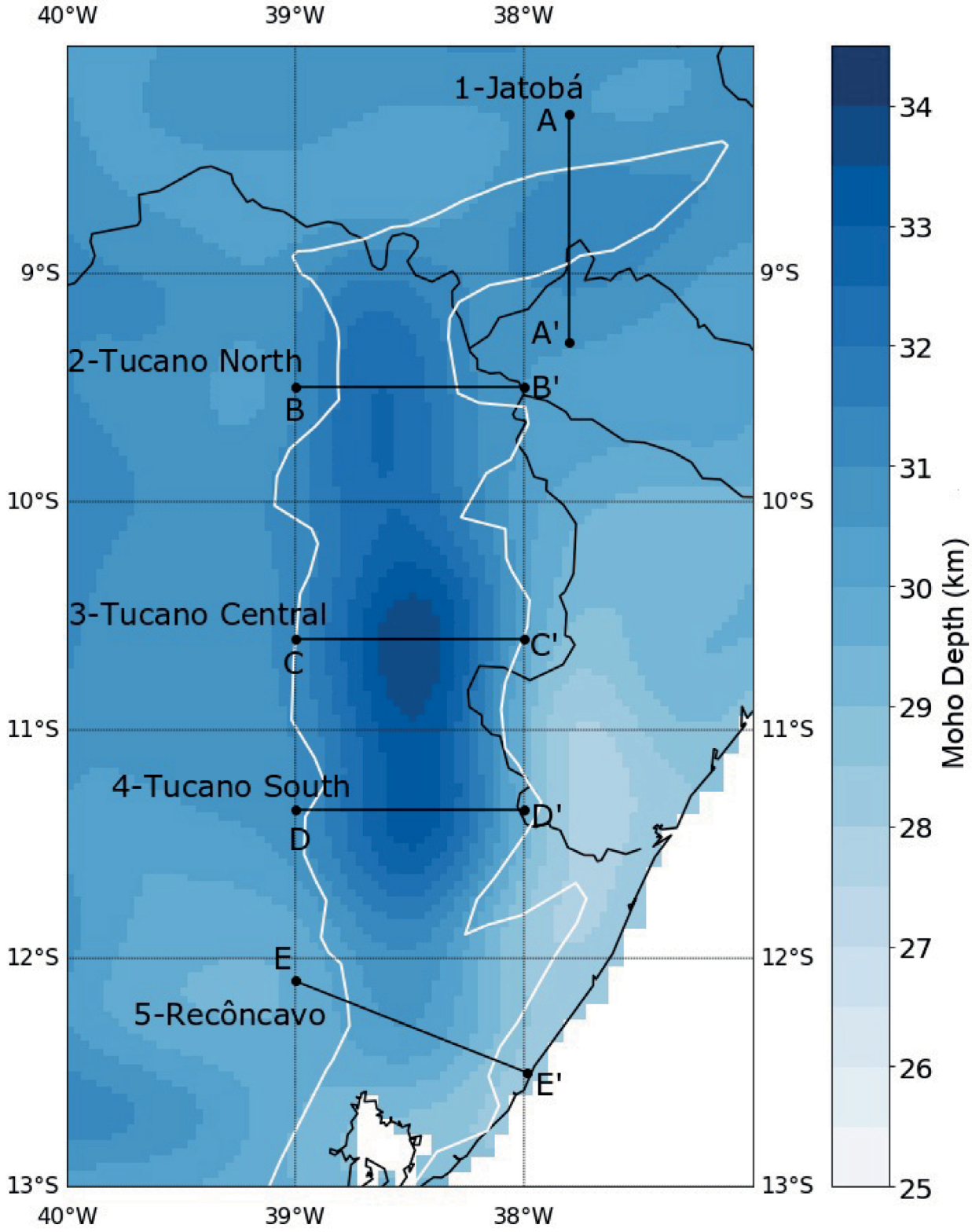


**Figure 6.** Moho 2D topography map in Recôncavo-Tucano-Jatobá rift-basin system. The color bar indicates the estimated depths in km.

modeling in this area and concluded that the rifting is compensated by elevation of the lithospheric mantle and melting of the crystalline crust.

In order to investigate the uniqueness of the crustal thickness map (Fig. 6), a large number of simulations were performed with a range of values for each of the input parameters, such as the initial average depth, the Moho interface density contrast, and the frequencies for the low-pass filter. The chosen method to select the initial average depth was according to the criteria used by van der Meijde *et al.* (2013), *i.e.* the initial average depth for Moho should be that of the expected crustal thickness for the area under investigation. The values ranged from 18 to 28 km, which are reasonable estimates, respectively, for oceanic and continental average crustal thickness.

Tests have shown that the best starting value for average depth is 26 km. However, a variation of 1 km in the initial average depth value implied a 1 km change in the estimated depths. Based on the most current models (van der Meijde *et al.* 2013), the average crustal depth in this region is 40 km.

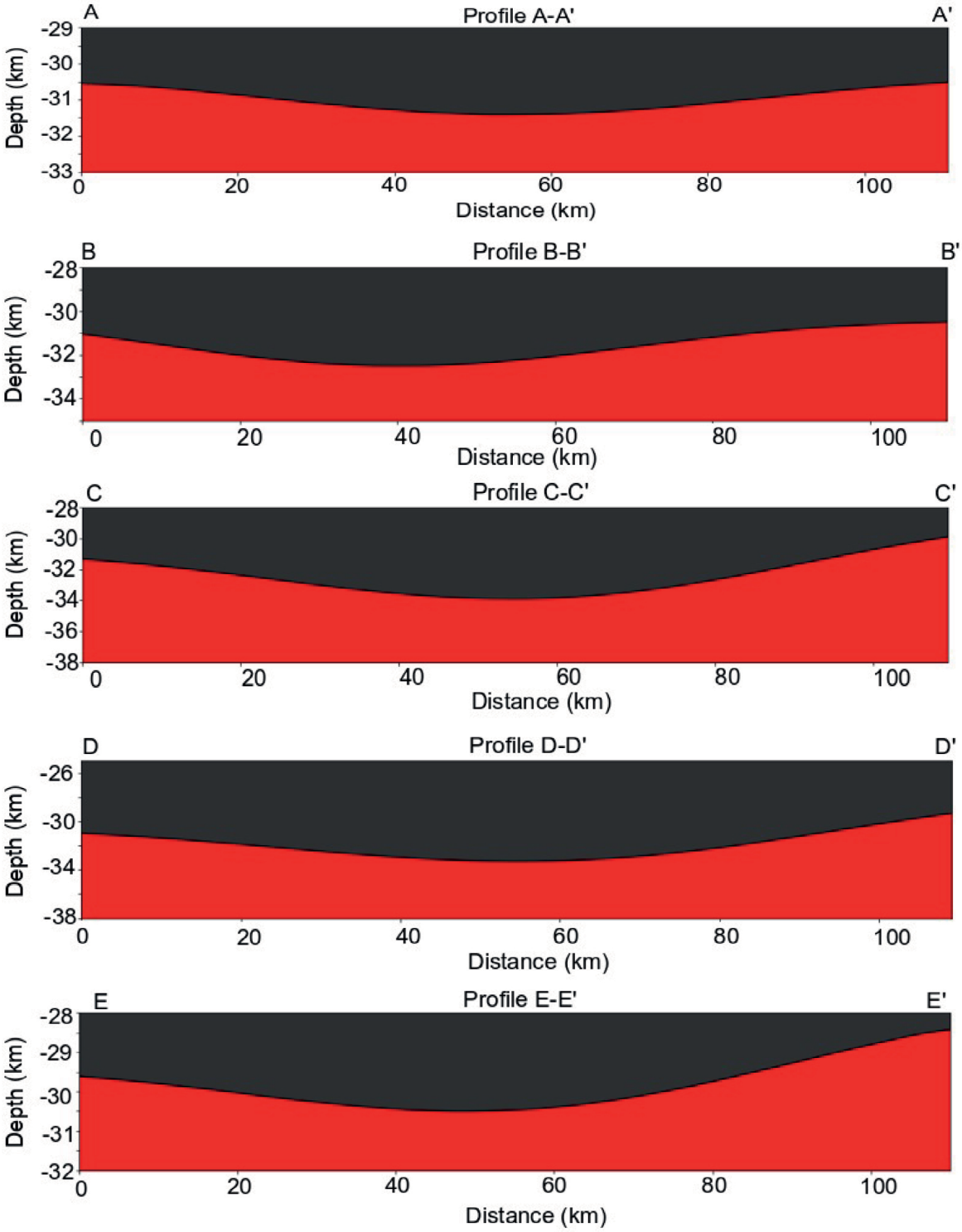


A – A': Jatobá Basin; B – B': North Tucano Sub-basin; C – C': Central Tucano Sub-basin; D – D': South Tucano Sub-basin; E – E': Recôncavo Basin.
**Figure 7.** Moho depth profiles under Recôncavo-Tucano-Jatobá rift-basin system.

The topography determination is obtained iteratively from the average depth value provided to the program, not depending on the zero depth, which is the surface of the earth. An increase in the density contrast value implies that the resulting topography remains close to the Earth surface, whereas a lower density contrast results in a thicker crust. Based on the work of Ussami *et al.* (1986) and Blaich *et al.* (2008), the density contrast of the crust/mantle interface in the studied region is 0.5 g/cm$^3$, whose value is used in the simulations of the present work.

By investigating the low-pass filter performance, we carried out a two-step analysis to define the selection criteria for the cutoff frequencies. In the first step, we had to generate the average radial power spectrum of the Bouguer anomaly data as a function of the wavelength, as shown in Figure 8. Its analysis allows the choice of the appropriate wavelength range for the separation between shallow and deep components, according to the technique of Spector and Grant (1970). These authors concluded that a set of anomalies with similar average depths have the same slope on the power spectrum curve. For the data set used in this paper, Figure 8 shows that the ideal wavenumber is 0.018 km$^{-1}$, *i.e.* it represents the junction point of two straight lines obtained by linear regression, in which these two straight lines approximately represent the full curve of the power spectrum. The left-hand straight line at this point is associated with low wavelength energies, *i.e.* larger and deeper sources. And the right-hand straight line to this point is associated with the energies of higher wavelengths, hence smaller and shallower sources. In the second step, the value of 0.018 km$^{-1}$ was used as a starting parameter, and variations were made around this value. Several estimators were used for comparative purposes. The first was the RMS deviation between the two last topography curves, as presented in Equation 5, which is called the *RMS* estimator. The number of iterations required, denoted by ITER, associated with the absolute RMS estimator *RMSE* and the average deviation, also absolute, called *MAE*, were recorded. The *RMSE*, in mGal unit, is defined as (Eq. 7):

$$RMSE = \sqrt{\frac{1}{n}\sum_{i=1}^{n} e_i^2} \tag{7}$$

And the *MAE*, also in mGal unit, is defined as:

$$MAE = \frac{1}{n}\sum_{i=1}^{n} |e_i| \tag{8}$$

being

$$e_i = Anomaly_{observed} - Anomaly_{calculated} \tag{9}$$

By space limitation, Figures 6 and 7 show only one result, with *RMS* = 0.013, *RMSE* = 14.4510 mGal and *MAE* = 9.9164 mGal. However, the most significant results were summarized in Table 1, which allowed us to draw some conclusions. Four values of $\Delta k = SH - WH$ were defined. For each defined $\Delta k$, there is an upper limit for *SH*, which we called $SH_{max}$, so that for $SH > SH_{max}$ the program needs more iterations to converge or it eventually does not converge. Basically, all the simulations are similar, and there is not many differences when comparing the depth maps visually. The results shown in Figures 6 and 7 used the parameters *WH* = 0.010 km$^{-1}$ and *SH* = 0.015 km$^{-1}$, which required three iterations.

**Table 1.** Comparative results for selection criteria of the filter cutoff parameters, *WH* and *SH*. The spatial frequency difference is given by $\Delta k = SH - WH$. (values in km$^{-1}$). The values of *RMS* are in km, and the values of *RMSE* and *MAE* are in mGal.

| $\Delta k$ | *WH* | *SH* | *RMS* | *ITER* | *RMSE* | *MAE* |
|---|---|---|---|---|---|---|
| 0.002 | 0.010 | 0.012 | 0.0010 | 3 | 14.5939 | 10.0544 |
| 0.002 | 0.016 | 0.018 | 0.0026 | 3 | 14.3976 | 9.8399 |
| 0.002 | 0.018 | 0.020 | 0.0030 | 3 | 14.4164 | 9.8207 |
| 0.005 | 0.010 | 0.015 | 0.0013 | 3 | 14.4510 | 9.9164 |
| 0.005 | 0.013 | 0.018 | 0.0022 | 3 | 14.3851 | 9.8425 |
| 0.005 | 0.016 | 0.021 | 0.0028 | 3 | 14.4088 | 9.8178 |
| 0.010 | 0.004 | 0.014 | 0.0134 | 2 | 15.3102 | 10.5640 |
| 0.010 | 0.008 | 0.018 | 0.0012 | 3 | 14.4778 | 9.9243 |
| 0.010 | 0.012 | 0.022 | 0.0023 | 3 | 14.3912 | 9.8211 |
| 0.016 | 0.001 | 0.017 | 0.0108 | 2 | 15.8388 | 10.9674 |
| 0.016 | 0.002 | 0.018 | 0.0132 | 2 | 15.3659 | 10.6011 |
| 0.016 | 0.008 | 0.024 | 0.0017 | 3 | 14.4219 | 9.8486 |

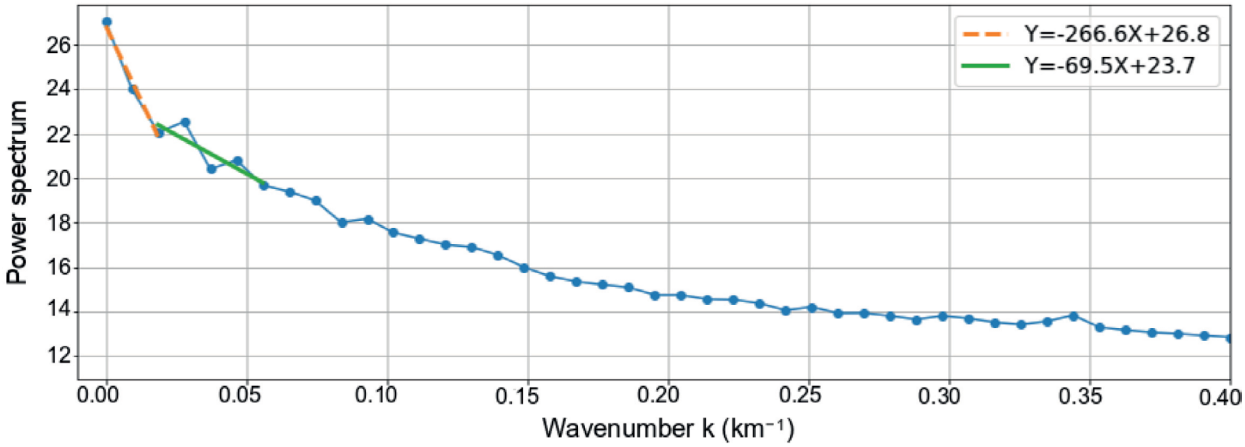


**Figure 8.** Average radial Bouguer anomaly power spectrum as a wavelength function.

We have computed the calculated anomaly field of Recôncavo-Tucano-Jatobá rift-basin system, which is presented in Figure 9, through forward modeling. When it was compared to Figure 5, we noticed that the two maps are very similar. In fact, the residual anomaly, which is the difference between the observed field and the calculated one, is displayed in Figure 10, in which it is possible to notice that most of the values fluctuate within the range plus/minus 4 mGal.

van der Meijde *et al.* (2013) inverted South American gravity data derived from the EIGEN-6C geopotential model, also based on the Parker-Oldenburg iterative algorithm. The crust thickness model, GMSA12, obtained by van der Meijde *et al.* (2013), follows the results of Assumpção *et al.* (2013). The GMSA12 model had better results when compared to other older models of crustal thickness for South America, especially in areas of difficult access for seismic surveys. The Moho topography model obtained in the present paper is in agreement with the values found by van der Meijde *et al.* (2013), as well as those provided in the GEMMA 1.0 (Reguzzoni and Sampietro 2015) and CRUST 1.0 (Laske *et al.* 2013) models.

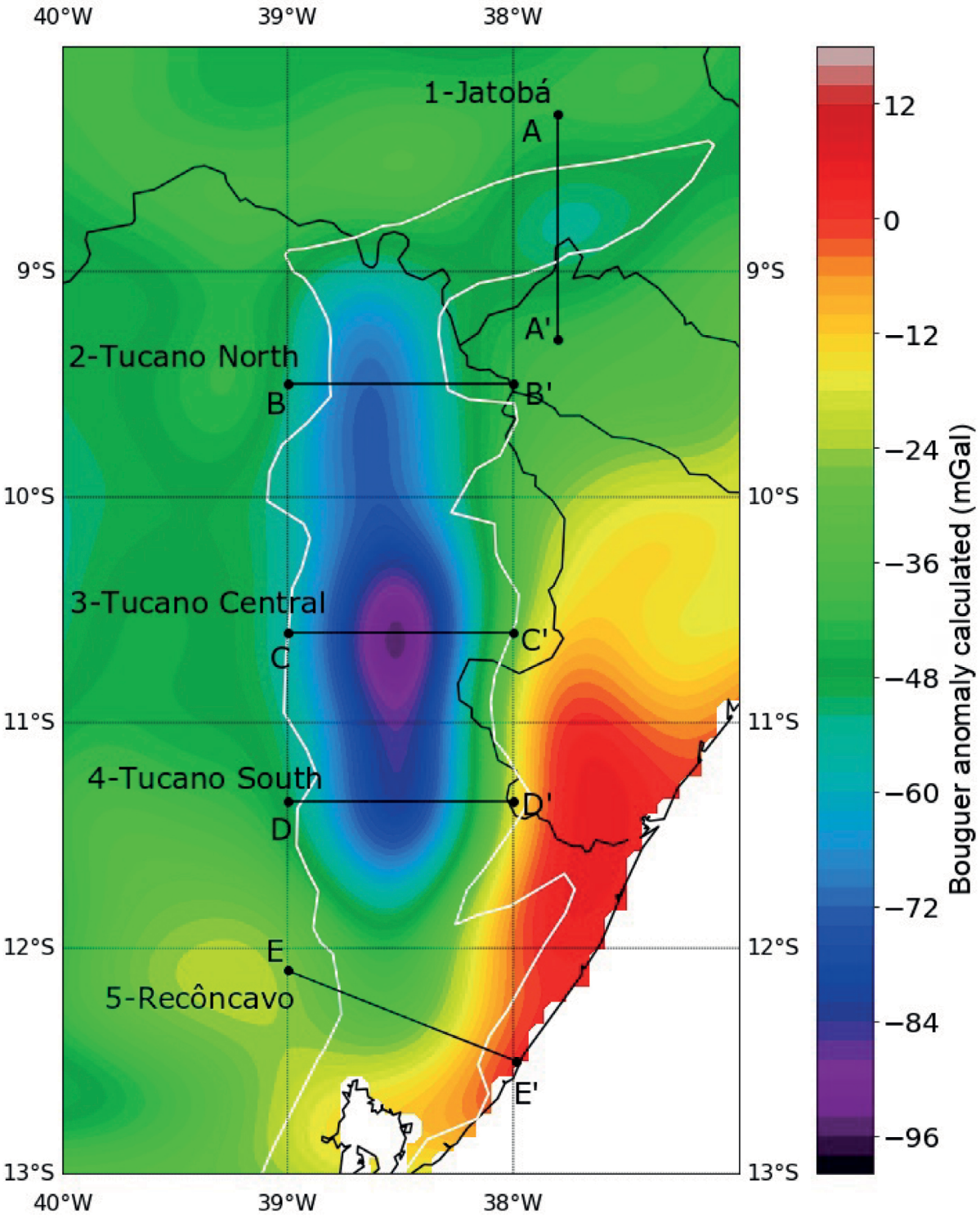


**Figure 9.** Calculated anomaly map of Recôncavo-Tucano-Jatobá rift-basin system.

In particular, the numerical comparison between our regional model and CRUST 1.0 indicated deviation below 10%, with the exception of the Jatobá Basin, in which the deviation was higher, but still under 15%. The CRUST 1.0 model is global, with a resolution of 1 × 1 degree, whereas the data sampling in our model was 2 × 2 minutes.

The Bouguer anomaly map in Figure 4 shows that all basins are characterized by large-scale negative gravity anomalies, indicating low-density sediment filling. There is no indication of positive anomalies caused by significant rise of Moho underlying the basin. Thus, these basins were not derived from a local isostatic compensation process; they were formed by the superior extension of the crust without complementary extension of the underlying rigid inferior crust and upper mantle.

The great rigidity at the time of basin formation implies that the rifting responsible for Tucano and Jatobá Basins was not associated with any significant modification of the thermal structure of the lithosphere immediately below. Ussami *et al.* (1986) analyzed the thermomechanical evolution of the same basins and concluded that McKenzie's simple model fails to

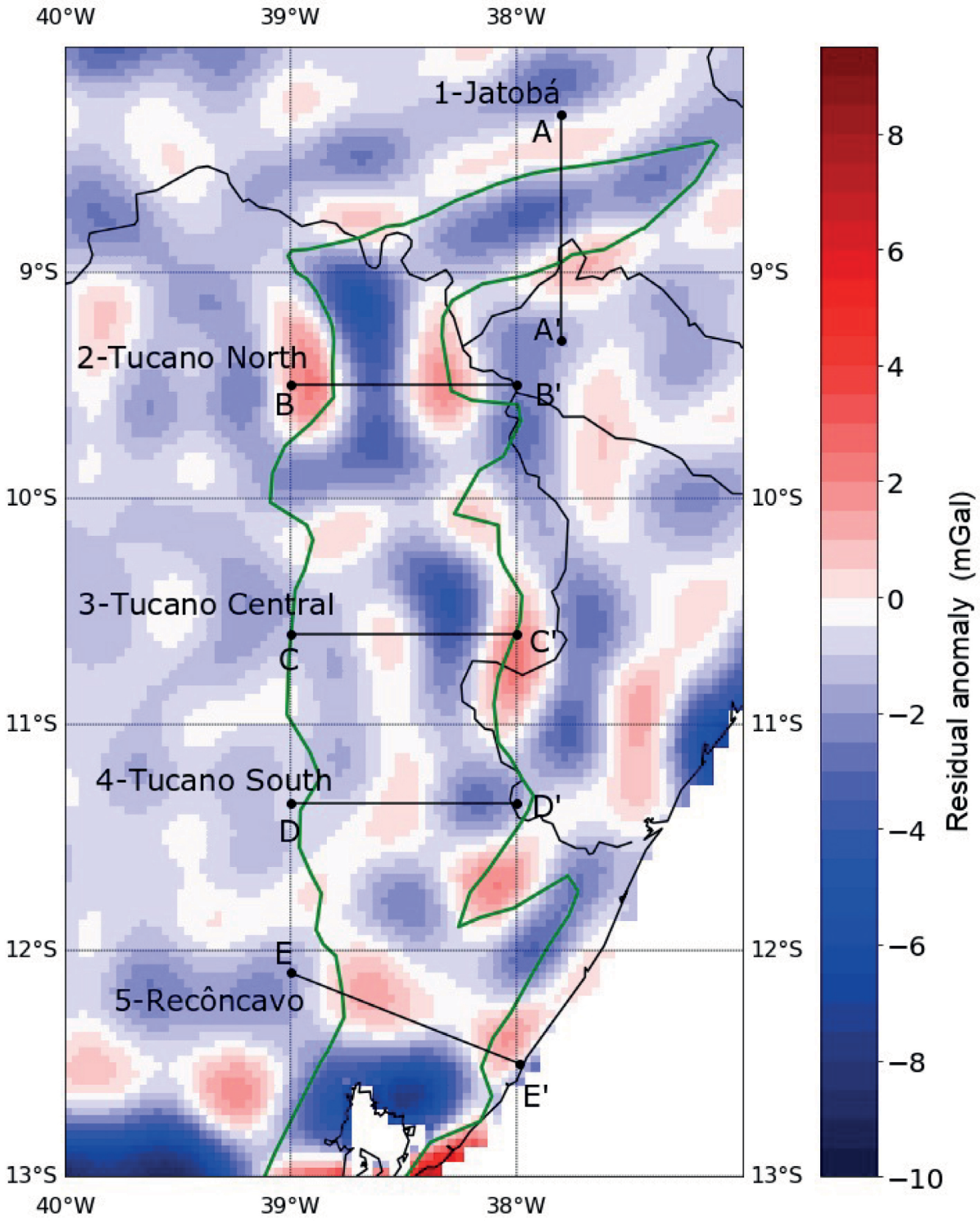


**Figure 10.** Residual anomaly map of Recôncavo-Tucano-Jatobá rift-basin system.

explain this coupled system of land and marine basins. All basins were suggested to be formed by a lithospheric extension during the rifting phase of the Atlantic division. The extension of the upper crust affected both land and marine basins, but the extent at deeper lithosphere levels, including the lower crust, was concentrated under the marine basins, as evidenced by the degree of thermal subsidence. Still according to Ussami *et al.* (1986), the origin of these land Brazilian basins is in accordance with Wernicke's simple shear model, in which the non-uniform crust extension is balanced by lower crustal and subcrustal lithospheric extension through a detachment surface.

Parker-Oldenburg routine was also applied to obtain the basement depths. For such procedure, the input data used in the previous inversion, that is, the upward continuation data that contains low frequencies, were subtracted from the Bouguer original data. The original data contain high and low frequencies, in such a way that the difference or the residual is associated with high frequencies. Its inversion provided the basement depth, as seen in Figure 11. The agreement between the

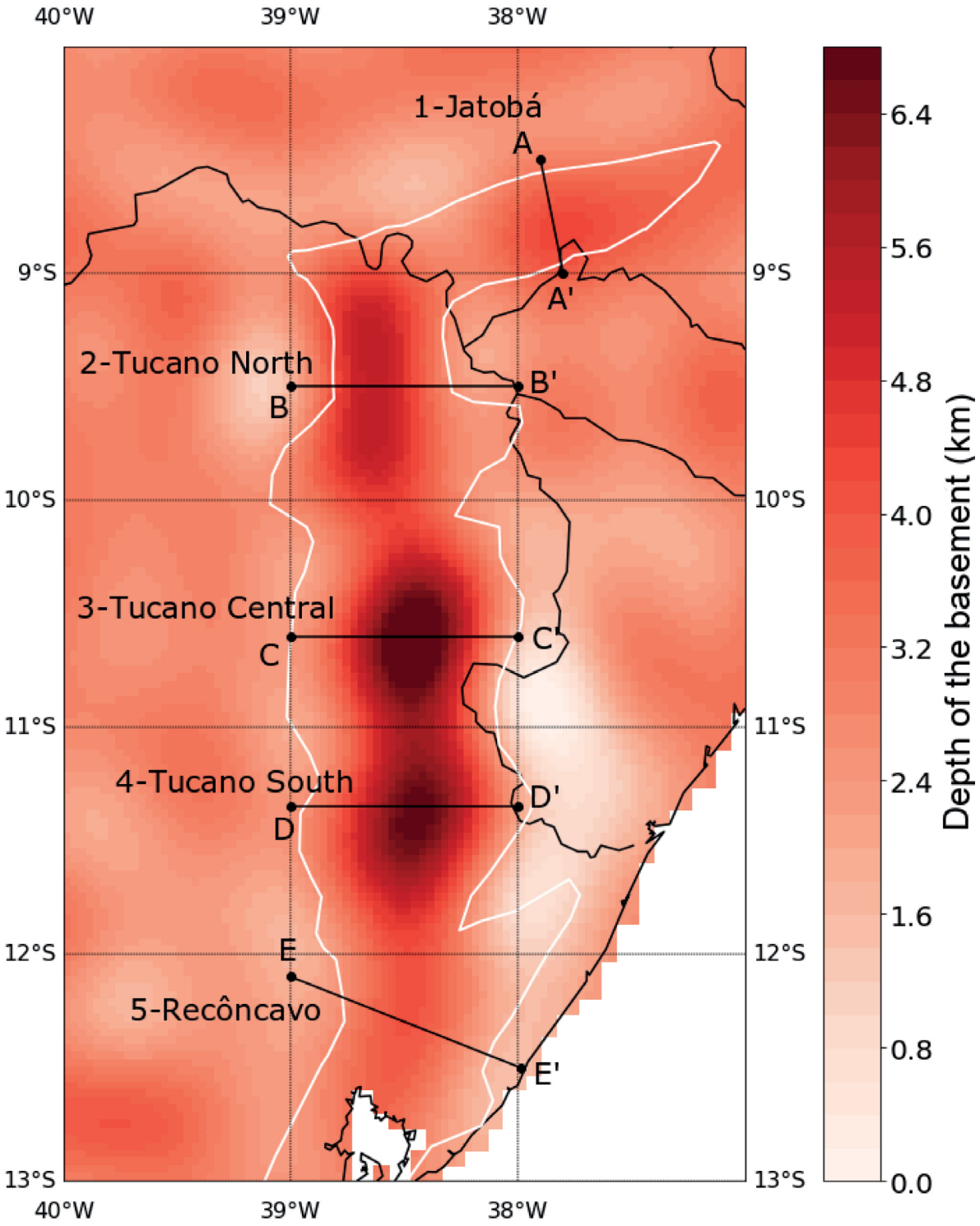


**Figure 11.** Basement topography map in Recôncavo-Tucano-Jatobá rift-basin system. The color bar indicates the estimated depths in km.

maximum depths, indicated in Figure 11 and those from the literature, is very consistent. For the Jatobá Basin, our result is 4,000 m that is equal to Magnavita (1992) estimate. For Tucano Sub-basins, we obtained 5,000 m in the North, 6,800 m in the Central and 6,000 m in the South, whereas the estimated values of Magnavita (1992) are, respectively, 6,000 m, 8,000 m and 6,000 m. For the Tucano Central Sub-basin, Santos *et al.* (1990) suggested 7,000 m. The exception in terms of agreement was Recôncavo Basin, in which Figure 11 suggests only 3,500 m, whereas the maximum thickness estimated by Magnavita (1992) is 6,900 m, and Santos *et al.* (1990) estimated 6,000 m. Recôncavo Basin has been shown to have a maximum crustal thickness of 29 km. In Tucano North Sub-basin, Moho appears to be close to 32 km. And finally, under the Jatobá Basin, the crust/mantle interface is around 30 km. The Moho topography model created here is in agreement with the values found by van der Meijde *et al.* (2013), by the model GEMMA 1.0 (Reguzzoni and Sampietro 2015), and also by the CRUST 1.0 model (Laske *et al.* 2013). Regarding the sedimentary package thickness, we inverted the high frequency anomaly field and the result, which are the basement depths, and they were consistent with the values found in literature.

## CONCLUSIONS

The models based on gravity data obtained from the algorithm of Gómez-Ortiz and Agarwal (2005) resulted in a unique continuity of crustal structure, providing new information about the structure and tectonics under the studied region. The interpretation of gravity anomalies allowed an estimate of the probable depth and shape of the causative body. The results showed that the Tucano Central Sub-basin has a thicker crust than the other basins, around 33 to 35 km, followed by the Tucano South Sub-basin, which is 33 km deep. In further South,

## ACKNOWLEDGMENTS

This paper was carried out with the support of *Coordenação de Aperfeiçoamento de Pessoal de Nível Superior – Brasil* (CAPES) — financing code 001. The authors also thank *Fundação de Amparo à Pesquisa do Estado da Bahia* (FAPESB) for project PIE00005/2016, Infrastructure Edict 003/2015. TP Bessoni thanks DM Novais for technical discussions and A. Bassrei thanks *Conselho Nacional de Desenvolvimento Científico e Tecnológico* (CNPq) for supporting *Instituto Nacional de Ciência e Tecnologia em Geofísica de Petróleo* (INCT-GP) project.

**ARTICLE INFORMATION**

Manuscript ID: 20190113. Received on: 10/21/2019. Approved on: 05/27/2020.

T.B. developed this study, inverted the gravity data, generated the figures, interpreted the results, and wrote the first version of the manuscript. A.B. supervised the research, translated the manuscript, contributed to the results discussion and to the text review. L.O. idealized and co-supervised the research.

Competing interests: The authors declare no competing interests.

## REFERENCES

Abrahão D., Warme J.E. 1990. Lacustrine and associated deposits in a rifted continental margin-lower cretaceous Lagoa Feia formation, Campos Basin, offshore Brazil. *In*: Katz B.J. (Ed.). *Lacustrine basin exploration:* case studies and modern analogs. AAPG Memoir 50, p. 287-305. https://doi.org/10.1306/M50523C18

Assumpção, M., Feng, M., Tassara, A., Julià, J. (2013) Models of crustal thickness for South America from seismic refraction, receiver functions and surface wave tomography. Tectonophysics, 609: 82-96. https://doi.org/10.1016/j.tecto.2012.11.014

Barthelmes F. 2009. *Definition of functionals of the geopotential and their calculation from spherical harmonic models, Scientific Technical Report STR09/02*. Postdam: GFZ German Research Centre for Geosciences. https://doi.org/10.2312/GFZ.b103-09026

Blaich O.A., Tsikalas F., Faleide J.I. 2008. Northeastern Brazilian margin: regional tectonic evolution based on integrated analysis of seismic reflection and potential field data and modeling. *Tectonophysics*, **458**(1-4):51-67. https://doi.org/10.1016/j.tecto.2008.02.011

Blakely R.J. 1996. *Potential theory in gravity and magnetic applications*. Cambridge: CUP, 464 p. https://doi.org/10.1017/CBO9780511549816

Braitenberg C., Zadro M., Fang J., Wang Y., Hsu H.T. 2000. The gravity and isostatic Moho undulations in Qinghai-Tibet plateau. *Journal of Geodynamics*, **30**(5):489-505. https://doi.org/10.1016/S0264-3707(00)00004-1

Cordell L., Henderson R.G. 1968. Iterative three-dimensional solution of gravity anomaly data using a digital computer. *Geophysics*, **33**(4):596-601. https://doi.org/10.1190/1.1439955

Dyrelius D., Vogel A. 1972. Improvement of convergency in iterative gravity interpretation. *Geophysical Journal International*, **27**(2):195-205. https://doi.org/10.1111/j.1365-246X.1972.tb05771.x

Ebbing J., Bouman J., Fuchs M., Lieb V., Haagmans R., Meekes J.A.C., Fattah R.A. 2013. Advancements in satellite gravity gradient data for crustal studies. *The Leading Edge*, **32**(8):900-906. https://doi.org/10.1190/tle32080900.1

Gómez-Ortiz D., Agarwal B.N.P. 2005. 3DINVER.M: a MATLAB program to invert the gravity anomaly over a 3D horizontal density interface by Parker-Oldenburg's algorithm. *Computers & Geosciences*, **31**(4):513-520. https://doi.org/10.1016/j.cageo.2004.11.004

Laske G., Ma Z., Masters G., Pasyanos M. 2013. *A New Global Crustal Model at 1x1 Degrees*. Available at: <https://igppweb.ucsd.edu/~gabi/crust1.html#download>. Accessed on: May 20, 2020.

Magnavita L.P. 1992. *Geometry and kinematics of the Recôncavo-Tucano-Jatobá Rift, NE Brazil*. PhD Thesis, University of Oxford, Oxford.

Magnavita L.P. 2000. Deformation mechanisms in porous sandstones: implications for development of fault seal and migration paths in the Recôncavo Basin, Brazil. *In*: Mello M.R., Katz B.J. (Eds.). *Petroleum systems of South Atlantic margins:* AAPG Memoir 73, p. 195-212.

Nagendra R., Prasad P.V.S., Bhimasankaram V.L.S. 1996. Forward and inverse computer modeling of a gravity field resulting from a density interface using Parker-Oldenburg method. *Computer & Geosciences*, **22**(3):227-237. https://doi.org/10.1016/0098-3004(95)00075-5

Oldenburg D.W. 1974. The inversion and interpretation of gravity anomalies. *Geophysics*, **39**(4):526-536. https://doi.org/10.1190/1.1440444

Paoletti V., Hansen P.C., Hansen M.F., Fedi M. 2014. A computationally efficient tool for assessing the depth resolution in large-scale potential-field inversion. *Geophysics*, **79**(4):A33-A38. http://dx.doi.org/10.1190/GEO2014-0017.1

Parker R.L. 1972. The rapid calculation of potential anomalies. *Geophysical Journal International*, **31**(4):447-455. https://doi.org/10.1111/j.1365-246X.1973.tb06513.x

Prates I., Fernandez R. 2015. *Bacia do Recôncavo:* sumário geológico e setores em oferta. Décima Terceira Rodada de Licitações. Brasil: Agência Nacional do Petróleo, Gás Natural e Biocombustíveis (ANP). Available at: <http://rodadas.anp.gov.br/arquivos/Round_13/areas_oferecidas_r13/Sumarios_Geologicos/Sumario_Geologico_Bacia_Reconcavo_R13.pdf>. Accessed on: May 20, 2020.

Reguzzoni M., Sampietro D. 2015. GEMMA: An Earth crustal model based on GOCE satellite data. *International Journal of Applied Earth Observation and Geoinformation*, **35**(Part A):31-43. http://dx.doi.org/10.1016/j.jag.2014.04.002

Sampietro D. 2015. Geological units and Moho depth determination in the Western Balkans exploiting GOCE data. *Geophysical Journal International*, **202**(2):1054-1063. https://doi.org/10.1093/gji/ggv212

Sampietro D., Sanso F. 2012. Uniqueness theorems for inverse gravimetric problems. *In*: Sneeuw N., Novak P., Crespi M., Sanso F. (eds.). *VII Hotine-Marussi Symposium on Mathematical Geodesy*. Heidelberg: Springer, p. 111-115. https://doi.org/10.1007/978-3-642-22078-4

Santos C.F., Cupertino J.A., Braga J.A.E. 1990. Síntese sobre a geologia das bacias do Recôncavo, Tucano e Jatobá. *In*: Raja Gabaglia G.P., Milani E.J. (eds.). *Origem e evolução de bacias sedimentares*. Rio de Janeiro: Petrobras, p. 235-266.

Silva I.C. 2017. *Evolução dinâmica do sistema de bacias tipo rift Recôncavo-Tucano-Jatobá com base em dados de campo.* PhD Thesis, Universidade Federal da Bahia, Salvador.

Sjöberg L.E. 2009. Solving Vening Meinesz-Moritz inverse problem in isostasy. *Geophysical Journal International*, **179**(3):1527-1536. http://dx.doi.org/10.1111/j.1365-246X.2009.04397.x

Spector A., Grant F. 1970. Statistical models for interpreting aeromagnetic data. *Geophysics*, **35**(2):293-302. https://doi.org/10.1190/1.1440092

Ussami N., Karner G.D., Bott M.H.P. 1986. Crustal detachment during South Atlantic rifting and formation of Tucano-Gabon basin system. *Nature*, **322**:629-632. https://www.nature.com/articles/322629a0

van der Meijde M., Julià J., Assumpção M. 2013. Gravity derived Moho for South America. *Tectonophysics*, **609**:456-467. https://doi.org/10.1016/j.tecto.2013.03.023